SCIENTIFIC REPORTS

OPEN

SUBJECT AREAS:
PATHOGENESIS
MINERALOGY

Received
24 June 2014

Accepted
9 December 2014

Published
16 January 2015

Correspondence and requests for materials should be addressed to G.-T.Z. (gtzhou@ustc.edu.cn)

Biomimetic synthesis of struvite with biogenic morphology and implication for pathological biomineralization

Han Li[1], Qi-Zhi Yao[2], Yu-Ying Wang[1], Yi-Liang Li[3] & Gen-Tao Zhou[1]

[1]CAS Key Laboratory of Crust-Mantle Materials and Environments, School of Earth and Space Sciences, University of Science and Technology of China, Hefei 230026, P. R. China, [2]School of Chemistry and Materials Science, University of Science and Technology of China, Hefei 230026, P. R. China, [3]Department of Earth Sciences, The University of Hong Kong, Hong Kong, P. R. China.

Recent studies have found that certain urinary proteins can efficiently inhibit stone formation. These discoveries are significant for developing effective therapies for stone disease, but the inhibition mechanism of crystallization remains elusive. In the present study, polyaspartic acid (PASP) was employed as a model peptide to investigate the effect of urinary proteins on the crystallization and morphological evolution of struvite. The results demonstrate that selective adsorption/binding of PASP onto the {010} and {101} faces of struvite crystals results in arrowhead-shaped morphology, which further evolves into X-shaped and unusual tabular structures with time. Noticeably, these morphologies are reminiscent of biogenic struvite morphology. Concentration-dependent experiments show that PASP can inhibit struvite growth and the inhibitory capacity increases with increasing PASP concentration, whereas aspartic acid monomers do not show a significant effect. Considering that PASP is a structural and functional analogue of the subdomains of aspartic acid-rich proteins, our results reveal that aspartic acid-rich proteins play a key role in regulating biogenic struvite morphology, and aspartic acid residues contribute to the inhibitory capacity of urinary proteins. The potential implications of PASP for developing therapeutic agents for urinary stone disease is also discussed.

Biologically controlled mineralization has been observed in many living organisms in nature. This creates various functional biominerals, such as mollusk shells, bones, teeth, and magnetosomes in magnetotactic bacteria[1–7]. Numerous investigations have revealed that some special acidic proteins play a major role in precisely controlling the formation of biominerals with unique morphologies[1,5,8,9]. On the contrary, pathological biomineralizations which include various diseases, such as urinary stones, gallstones, and atherosclerosis[10–14], lack biological control. To conquer these diseases, researchers have made great efforts to reveal the mechanisms of stone formation, and have found that many natural modulators have a stimulatory or inhibitory influence on the crystallization and retention of stones in body fluids[15–22]. The most potent modulators are proteins enriched in acidic amino acid residues, such as aspartic or glutamic acids[16,18,21–24].

Among the pathological stones, urinary stones, which have been plaguing human beings since the beginning of civilization[25] are vitally important, causing symptoms in 3–20% of people throughout the world with a recurrence rate of 50%[26]. The main constituents of urinary stones are calcium oxalate, calcium phosphate, struvite, uric acid, and cysteine[10]. Struvite, known as magnesium ammonium phosphate hexahydrate ($NH_4MgPO_4 \cdot 6H_2O$), crystallizes in the orthorhombic system and accounts for 15 to 20% of all urinary stones[10]. The formation of struvite is associated with a urinary tract infection by urease-producing microorganisms, including *Proteus mirabilis*[10,11,27], which occurs because urease can split urea into carbon dioxide and ammonia. Generated ammonia increases the urinary pH, which leads to an elevation of the concentration of NH_4^+, CO_3^{2-}, and PO_4^{3-}. These ions subsequently combine with Mg^{2+} cations present in urine to precipitate struvite.

Struvite formation is among the most difficult and dangerous conditions in stone disease as it can rapidly grow in human body with a high degree of recurrence and presents the damaging appearance of a "staghorn"[11,28–32]. In vitro experiments also found similar dendrites when struvite was formed in synthetic urine in the presence of *Proteus mirabilis*[26,33]. Such staghorns and dendrites can easily remain to form larger stones and at the same time damage the epithelium of the internal renal walls[26]. The affected areas can in turn serve as nucleation sites for struvite crystallization, promoting the crystal growth and aggregation of struvite[26]. Therefore, it is the crystal morphology that creates a vicious circle for stone formation and makes struvite a more painful urological disorder

in human body. In addition to the staghorn-like and dendritic morphologies, biogenic struvite also presents other special features, such as X-shaped and unusual tabular habits (with an 'X' on the surface), which are significantly different from their abiotic counterparts[27,33–38].

In view of these special morphologies and their disadvantages, struvite morphogenesis has been increasingly recently investigated using two principal methodologies. The first approach explores the metabolic effects on the morphology of struvite crystals in the media of urease-producing microorganisms isolated from infectious stones[26,27,33,35,37–39]. The second approach is based on biomimetic model systems, and examines the influence of biological macromolecules and synthetic polymers on crystal morphogenesis[29,36,40,41]. In the first approach, it is presumed that these special morphologies depend on either supersaturation or growth kinetics. For example, Mclean et al. noted that the crystal habit of struvite varies markedly according to the growth rate[35]. That is, high growth rates lead to elongation along one or two crystal planes, inducing the appearance of dendritic or X-shaped crystals. When the growth rate slows down, tabular crystals develop. Prywer and Torzewska also observed X-shaped and dendritic morphologies during the mineralization of struvite crystals with *Proteus* bacteria in synthetic urine[27]. They suggested that these morphologies are caused by heterogeneous distribution of supersaturation around the growing crystals, which is highest at the corners and edges and lowest at the center of a given crystal surface. Recently, Prywer et al. reported that high supersaturation might change the tendency of primary crystals to form rhombohedra, which are well aligned and arranged layer-on-layer to form the X-shaped structures[33]. Using the second approach, investigators have found that some proteins, such as calprotectin, albumin and immunoglobulins, might inhibit the growth of struvite[36,40]. Moreover, Asakura et al. observed X-shaped morphology when they tested the effect of calprotectin on urease-induced struvite growth in artificial urine[36]. These findings raised further questions, e.g., whether there is a close relationship between urinary proteins and biogenic struvite morphologies, and why some urinary proteins can inhibit struvite growth.

Herein, polyaspartic acid (PASP) was chosen as a model biological additive to influence the crystallization and growth of struvite, and an ammonia diffusion technique was used to synthesize struvite, which might emulate the biomineralization of struvite *in vivo*. The goal of this study was to examine the effect of PASP on the growth and morphological development of struvite and to reveal the morphogenetic mechanism of biogenic struvite. Our results showed that in the presence of PASP, struvite with biogenic structures can be crystallized, and a series of time-resolved experiments revealed that struvite crystals experienced a significant morphologic evolution from arrowhead-shaped through X-shaped to unusual tabular habits (with an 'X' on the surface). A plausible mechanism for the morphogenesis of hierarchical struvite crystals was proposed. Remarkable reductions in struvite dimensions and total mass were also observed with a continuous increase in PASP concentration, which may explain why a number of urinary proteins acted as stone growth inhibitors in urine, leading to a better understanding of pathological biomineralization and the application of PASP to lithiasis treatment.

Results

In order to understand the effect of PASP on the morphological evolution of struvite, a series of time-resolved mineralization experiments from 20 min to 20 h was carried out at PASP concentrations of 0 and 0.2 mM, respectively. The composition and phase purity of the products were first examined by the XRD technique, and the results confirm that all of the mineralized products are orthorhombic struvite with space group $Pmn2_1$. The representative XRD patterns for the products obtained with and without PASP are shown in Figure 1a–c. Compared with the standard diffraction pattern of struvite (in Figure 1, JCPDS file No.15–0762), all of the diffraction peaks could be well indexed as struvite, and no other impurity phases could be found. At the same time, it is not difficult to find from Figure 1a–c that the products obtained in the presence of PASP had dramatically strong (020) and (040) diffractions, indicating that the mineralized products were preferentially oriented along the [010] direction. Moreover, FT-IR analysis has also been proved to be a valuable method to distinguish the different phases and compositions[42]. Therefore, FT-IR analyses were performed on the mineralized products. The typical FT-IR spectra of the mineralized products with and without PASP are depicted in Figure 2. The absorption bands located at 1007, 572 and 462 cm^{-1} can be assigned to the PO_4^{3-} antisymmetric stretch (ν_3), the P-O bend (ν_4) and the PO_4^{3-} ν_2 modes, respectively. The absorption bands at 1469, 1435 and 1400 cm^{-1} can be attributed to ν_4 (NH_4^+) antisymmetric bending. Water-water H bonding at 761 cm^{-1} and ammonium-water H bonding at 892 cm^{-1} can also be recognized from this FTIR spectrum. These are in good agreement with the results for pure struvite reported by Banks et al.[42], further confirming that the mineralized products are struvite. Therefore, the XRD and FT-IR results reveal that pure phase of struvite can always be obtained in the presence and absence of PASP, and dissolved PASP in the mineralization solution does not influence the phase composition of the mineralized products. Moreover, the characteristic vibrational bands [band of ν (C = O) in amide group at approximately 1645 cm^{-1}, band of ν (C = O) in carboxylic group near 1731 cm^{-1}, band of ν (C-H) in methylene group at approximately 2969 and 2904 cm^{-1}] belonging to PASP molecules[43] do not appear in Figure 2a, suggesting that no detectable content of PASP is occluded in the mineralized product after extensive washing.

The morphology and textures of the mineralized products were further observed by FESEM. In the presence of 0.2 mM PASP, a range of struvite crystals with different morphologies was obtained at different mineralization durations, as shown in Figure 3, panels a1–f1. At 20 min, very little sample is obtained, mainly containing crystals with an arrowhead-shaped morphology with a mean dimension of ca. 10 μm (Figure 3, panel a1). It appears that the arrowhead-like crystals exhibit typical hemimorphic morphology, that is, the two ends of a crystallographic *c*-axis are not related by symmetry[27]. It is well known that struvite has an orthorhombic structure with space group $Pmn2_1$. Therefore, the arrowhead-like crystal can be described as a crystallographic combination consisting of the {001}

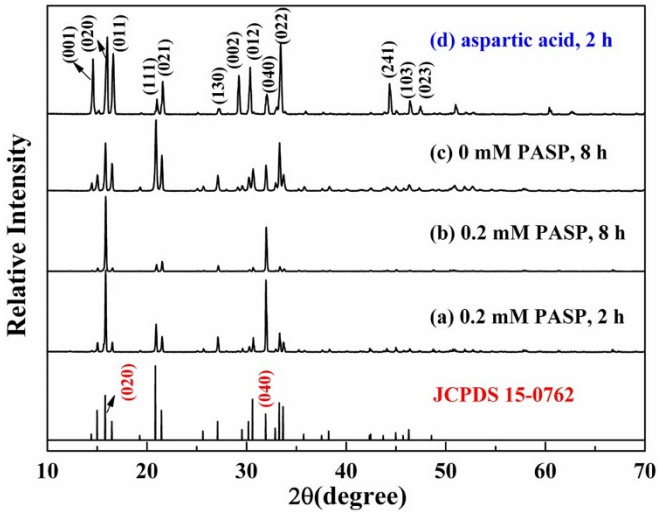

Figure 1 | Representative XRD patterns of the samples grown for 2 h with 0.2 mM PASP (a), 8 h with 0.2 mM PASP (b), 8 h without PASP (c), 2 h with aspartic acid (d), and the standard XRD pattern for struvite (JCPDS file No. 15–0762).

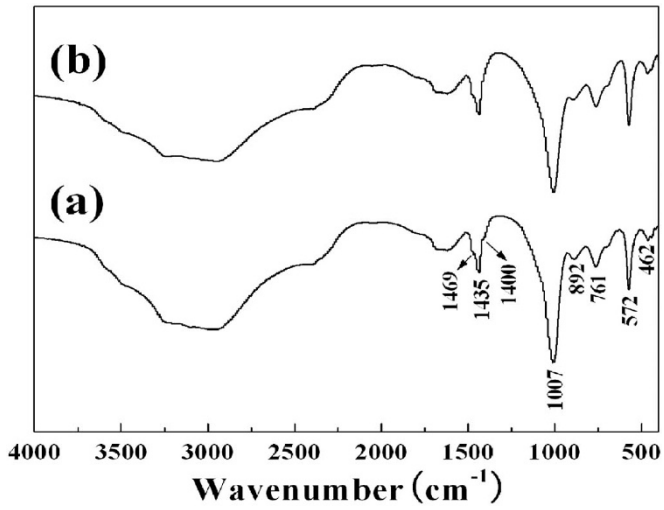

Figure 2 | FTIR spectra of the products grown for 8 h with 0.2 mM (a) and 0 mM (b) PASP.

and {00-1} pedions, the {101}, {01-1}, {10-1} and {011} domes, and the {010} pinacoid, as illustrated in Figure 3, panel a1. After 1 h of mineralization, a few more crystals are generated and the morphology exhibits a quadrangular tabular habit with a length of ca. 30 μm and a width of ca. 20 μm (Figure 3, panel b1). Nevertheless, the striations and voids left on the quadrangular tabular structures indicate that the tabular architectures are assembled from four arrowhead-shaped crystals. The quadrangular tabular architecture is almost 4 times as large as the arrowhead-shaped structure, further supporting that an assembly process might occur. Furthermore, FIB/SEM analyses show that the middle of cross section in the architecture has a much rougher and porous appearance (see Supplementary Fig. S1d online), which reveals that the fusion and topotactic growth are incomplete in the boundary of subunits, confirming that the quadrangular tabular structures form from a self-assembly of the arrowhead-like subunits. The quadrangular tabular structures were further characterized by the TEM and SAED techniques. Unfortunately, no TEM image and SAED pattern for the architectures is available due to the quick melting and decomposition of struvite under the bombardment of the electron beam. In fact, our TG–DTA analyses also indicate that struvite easily loses its six water molecules and an ammonia molecule at lower temperatures (see Supplementary Fig. S2 online). At a mineralization time of 2 h, the X-shaped structures are observed, as shown in Figure 3, panel c1. The four extended angles in the X-shaped structures reveal that the preferential growth occurs along the <001> direction of every assembled subunit. This characteristic X shape has been reported by several researchers when struvite crystallized in the presence of urease-producing bacteria[26,27,33,35,37,38]. After 3 h of mineralization, the X-shaped crystal develops a more tabular appearance with the void spaces gradually filled by the peripheral growth, leaving an 'X' on the top surface (Figure 3, panel d1). Prolonging mineralization time to 8 h leads to the appearance of unusual tabula-like structures with a length of ca. 80 μm and a width of ca. 30 μm, and almost all of the tabulae are truncated (Figure 3, panel e1). Additionally, it can clearly be seen that there is an 'X' on the top surface while the opposite side is flat. This unusual tabular habit is similar to the biogenic struvite morphology reported by Mclean et al., Prywer and Torzewska, and Zhu et al.[35,37,38]. At a mineralization time of 20 h, regrowth and/or Ostwald ripening blur the 'X' on the surface of the unusual tabular struvite, resulting in a flatter tabular morphology, with a length of ca. 100 μm and a width of ca. 30 μm (Figure 3, panel f1). However, in the absence of PASP, only the rod-shaped or long tabular crystals are harvested with a length of hundreds of micrometers, as depicted in Figure 3, panels a2–f2. Specifically, panels a2 and b2 in Figure 3 show that the products mineralized for 20 minutes and 1 h consist mainly of rod-shaped crystals. At a mineralization duration of 2 h, some rod-like crystals develop into penniform-like structures with saw-toothed sides (Figure 3, panel c2). After 8 h of mineralization, the long tabular habits dominate the crystal's appearance (Figure 3, panel e2). A further extension of the mineralization time to 20 h leads to the huge tabular habit (Figure 3, panel f2). Concisely, a series of time-course experiments with and without PASP revealed that PASP plays an important role in the specific morphogenesis of struvite.

Moreover, in order to better understand the effect of PASP on struvite crystal growth, mineralization experiments with different concentrations of PASP were also carried out, and a 2 h mineralization time was deliberately chosen because our time-resolved experiments indicated that the orientation aggregation/assembly of the struvite subunits occurs between 1 and 2 h (Figure 3, panels b1 and c1). In the absence of PASP, a large number of long penniform crystals was obtained, with a length of ca. 190 μm (e.g., Figure 3, panel c2). However, when 0.1 mM of PASP was added, the product had a large X-shape with a length of ca. 100 μm, and some attached grains forming two intersecting lines on the surface could also be seen (Figure 4a). If the PASP concentration was increased to 0.2 mM, the X-shapes still dominated the crystallization habits, but the lengths were reduced to 50 μm (e.g., Figure 3, panel c1). At a PASP concentration of 0.4 mM, both X-shaped and short tabular habits coexisted, with a length of ca. 30 μm and ca. 20 μm, respectively (Figure 4b). When the PASP concentration reached 0.8 mM, all of the crystals had a short tabular habit and the mean length was 20 μm (Figure 4c). However, further increasing PASP concentration to 2 mM did not lead to a remarkable change in the shape and size of struvite (Figure 4d), only a reduced output. In order to unambiguously demonstrate the dependence of the yield and dimensions of the mineralized struvite on PASP, all trials were conducted five times to calculate a mean yield, and 30 particles from the SEM images were measured in each case to determine an average length. As shown in Figure 5, either the yield or dimensions of struvite dramatically decreases with an increase in the PASP concentration. Although the inhibitory effect on the dimension was tested at saturation after the addition of 0.8 mM of PASP, the yield of struvite consistently and dramatically decreases. It appears that PASP not only significantly impacts the morphology of struvite but also effectively inhibits the nucleation and growth of struvite.

Discussion

PASP has been widely used as a model peptide to understand the interaction between biomineralization-associated acidic proteins and minerals such as calcium carbonate, calcium oxalate, calcium hydrogenphosphate dehydrate, and octacalcium phosphate[18,44–48]. Moreover, PASP has also been documented as an excellent inhibitor to effectively inhibit crystal growth of calcium carbonate, calcium sulfate, calcium oxalate, calcium phosphate, and barium sulfate salts[46,48–54]. It is generally believed that its inhibitory effect could be achieved in two ways. On the one hand, PASP could selectively bind to some specific crystal faces by its carboxyl chains and hence decrease their growth rates[44,46,48,52]. On the other hand, PASP could serve as an excellent chelating agent, thus forming stable complexes with various metal cations in solution[55–57], in which the activity of the free metal cations would be significantly reduced to restrain the growth of crystal.

Our time-resolved experiments show that in the presence of PASP, struvite exhibited different morphologies over time, including arrowhead-shaped, X-shaped and unusual tabular morphologies (Figure 3), and the arrowhead-like structures might act as the primary assembled subunits of the X-shaped and unusual tabular structures. However, in the absence of PASP, 20 min of mineralization

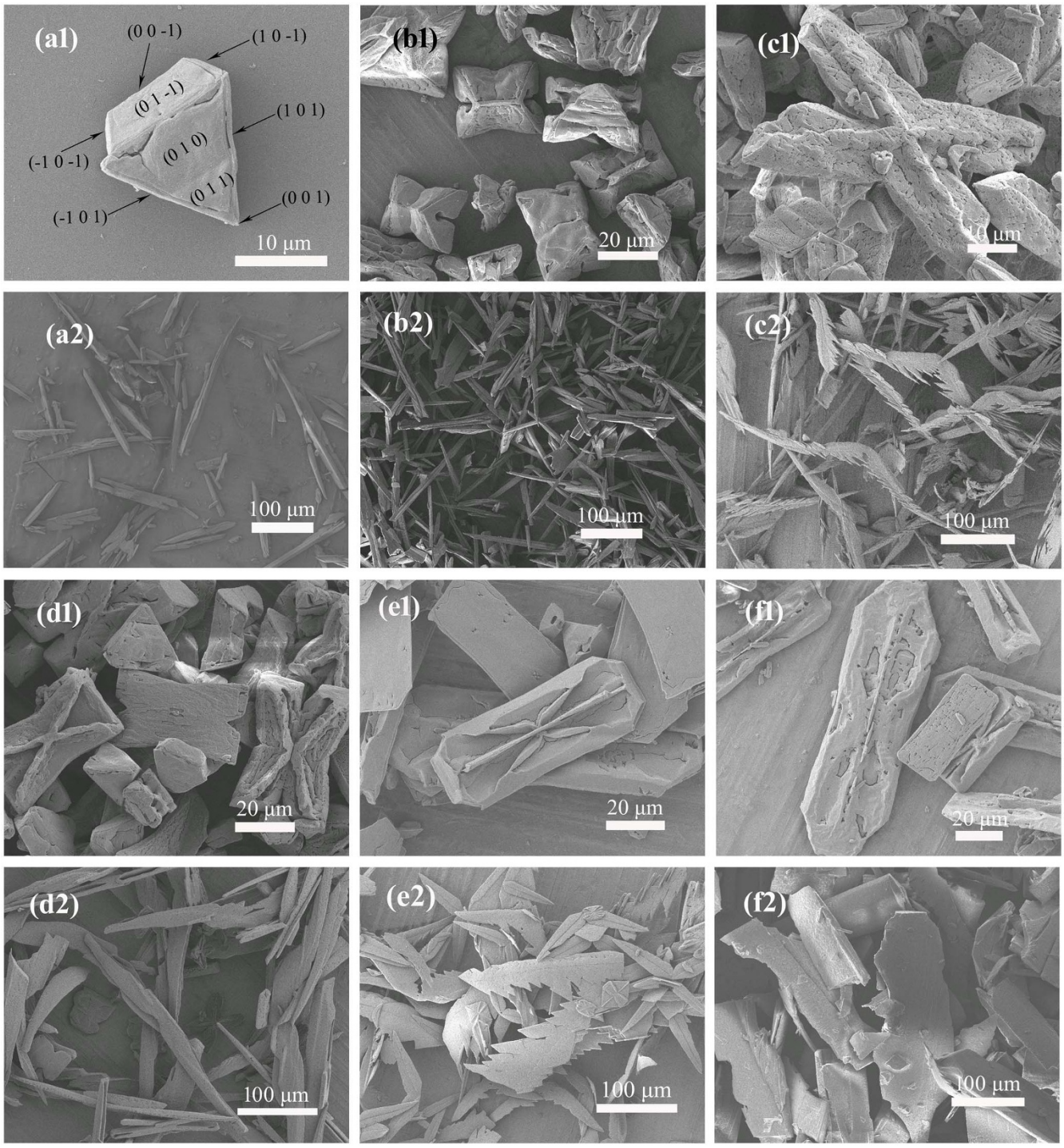

Figure 3 | FESEM images of struvite crystals synthesized for 20 min (a1, a2), 1 h (b1, b2), 2 h (c1, c2), 3 h (d1, d2), 8 h (e1, e2) and 20 h (f1, f2) with 0.2 mM PASP and without PASP, respectively.

only leads to rod-like or long tabular crystals, while no arrowhead-like struvite can be found (Figure 3, panel a2). This indicates that the PASP molecules are likely responsible for the formation of the special arrowhead-like subunits. Wierzbicki et al. also obtained arrowhead-shaped crystals when they examined the inhibitory effect of phosphocitrate on struvite crystal growth[58]. They suggested that phosphocitrates preferentially binding to {101} faces lead to an enhanced expression of these faces, thus modifying the crystal morphology. In our case, the arrowhead-shaped crystals have preferably developed {101}, {010} and {01-1} faces (e.g., Figure 3, panel a1). This indicates that the preferential adsorption and binding of PASP onto these faces occurs and results in the prominent development of these faces. Molecular simulations by Wierzbicki et al. and Romanowski et al. have shown that the {101} and {010} faces of struvite have high density of magnesium cations coordinated with water molecules[31,58]. Our molecular modeling results also showed that the well-developed {101} and {010} faces have a much higher density of Mg^{2+} than the less developed {011} faces (see Supplementary Fig. S3 and S4 online). These crystal faces with a high Mg content could provide a positively charged environment for the preferential adsorption and binding of negatively charged species. PASP molecules contain a large number of negatively charged carboxyl side chains. Therefore, strong electro-

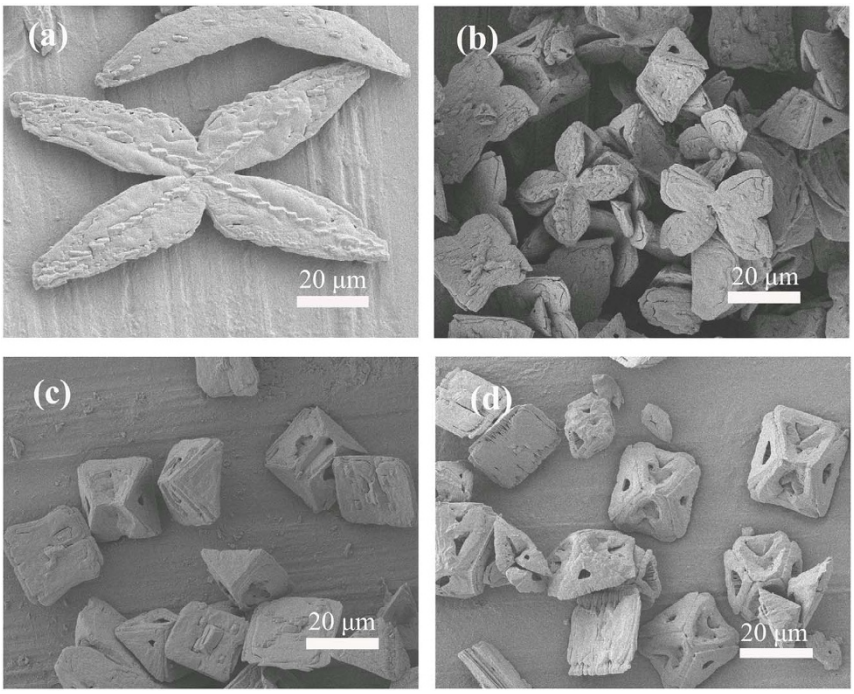

Figure 4 | **FESEM images of struvite crystals grown for 2 h with 0.1 mM (a), 0.4 mM (b), 0.8 mM (c) and 2 mM (d) PASP.**

static interactions occur between PASP molecules and the {101} and {010} faces. The decrease of growth rate in turn leads to an enhanced expression of the {101} and {010} faces. Other faces with a low density of magnesium cations or the presence of negatively charged phosphate groups will cause a lack of attraction for PASP, and grow faster. For example, the (011) face with lower density of Mg^{2+} shows reduced expression in the arrowhead-shaped morphology (e.g., Supplementary Fig. S4 and Figure 3, panel a1). Moreover, the XRD analyses (Figure 1a and b) also show that the products obtained in the presence of 0.2 mM PASP after 2 and 8 h of mineralization have much stronger (020) and (040) diffractions relative to the standard pattern of struvite (JCPDS file No.15-0762), further confirming the existence of the well-developed {010} faces.

After arrowhead-shaped struvite forms, every four arrowhead-shaped crystals further self-assemble into quadrangular tabular architecture (Figure 3, panel b1). Here, the driving force controlling the self-assembly process may result from long-range dipole-dipole interactions between the assembled units[33,59,60]. As described by Prywer et al., the (001) face in struvite is rich in NH_4^+ groups, while (00-1) face is rich in PO_4^{3-} and $Mg(H_2O)_6^{2+}$ groups[33]. As a result, the *c* axis is the dipole axis. Therefore, the intrinsic dipole-dipole interactions from the arrowhead-shaped crystals should drive them to orient and attach along coherent crystallographic directions, forming quadrangular tabular architectures (e.g., Figure 3, panel b1). With the further prolongation of the mineralization duration, the assembled tabular architectures continue growing along the <001> direction with a relatively high growth rate, resulting in the X-shaped morphology (Figure 3, panel c1). Subsequently, the peripheral growth gradually fills the voids in the X-shaped structures, and the X-shaped morphology evolves into unusual tabular habits with an 'X' on the top surface (Figure 3, panel e1). Finally, the Ostwald ripening process smoothens the surface and the conspicuous 'X' disappears (Figure 3, panel f1).

Taken together, our time-resolved experiments indicate that in the presence of PASP, a significant morphological evolution of struvite occurs from the arrowhead-like shape through the assembled

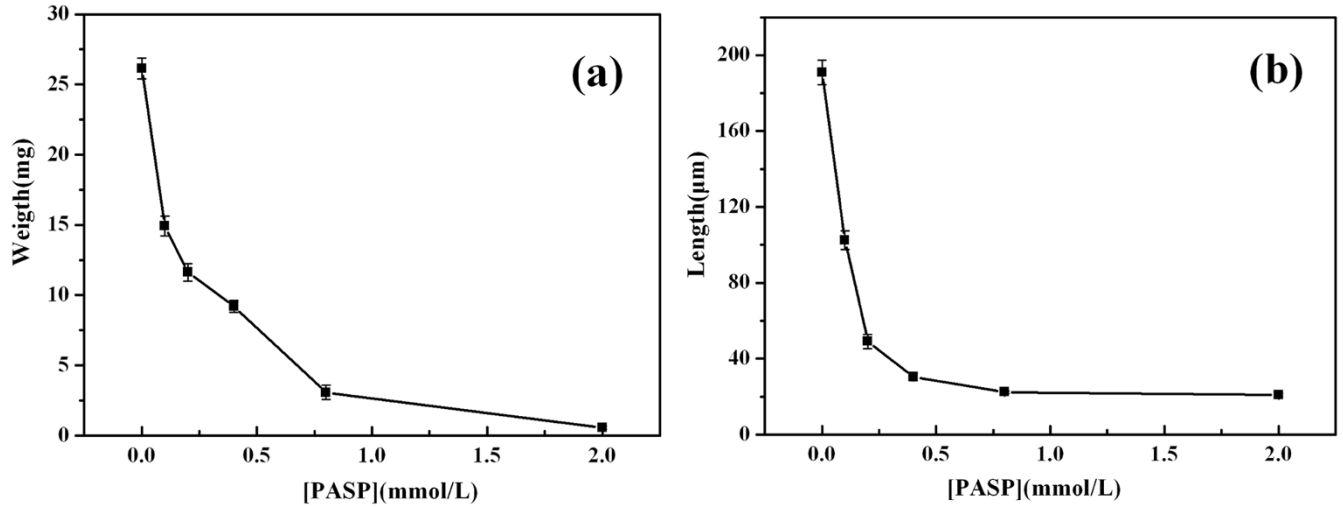

Figure 5 | **Relationship between PASP concentrations and weight (a) or length (b) of struvite obtained in the concentration-dependent experiments.**

quadrangular tabular architecture, the X-shape, and the unusual tabula to the flatter tabular structure with a blurred X on its surface. Such process can be clearly illustrated in Figure 6, and be achieved by a train of steps, including the selective adsorption/anchoring of PASP molecules, oriented attachment and fusion of the subunit, orientation growth, peripheral growth, and Ostwald ripening. Among these obtained shapes, the X-shaped and unusual tabular habits resemble biogenic morphologies of struvite. This suggests that biogenic X-shaped and unusual tabular struvite may represent two different growth stages, and that the aspartic acid-rich urinary proteins can be responsible for the specific morphogenesis of biogenic struvite. In the other words, biogenic struvite morphology can be developed under the control of urinary proteins, and the biogenic X-shaped and unusual tabular habits are the metastable growth forms of the biogenic struvite. Therefore, our results can provide a new insight into the biological origin of struvite with a variety of morphologies.

PASP concentration is another important factor for the crystal growth of struvite. Without PASP, struvite grows rapidly and a mass of penniform crystals with a length of ca. 190 μm are obtained (Figures 3 and 5). However, when 0.1 mM of PASP is added, struvite shows a regular X-shape and the crystal size is nearly halved. Further increasing the PASP concentration results in a decrease of crystal size and yield (Figures 4 and 5). These results indicate that PASP can also effectively inhibit struvite growth in solution. It has been reported that metal cations complex with PASP to form metal−PASP species because PASP contains a mass of carboxyl groups[55,57]. Therefore, PASP molecules can tightly combine with Mg^{2+} to form magnesium-PASP complexes, resulting in the effective growth inhibition of struvite.

Moreover, our experiments using aspartic acid instead of PASP show that in the presence of aspartic acid, plenty of long irregular tabular struvite crystals (Figure 7) can be obtained (the XRD shown in Figure 1d). This shows that the aspartic acid monomer cannot exert a similar influence on the specific morphogenesis and growth inhibition of struvite as PASP in spite of the same stoichiometry of their respective carboxyl groups. Similar results have also been observed in the interactions between aspartic acid and other minerals, such as calcium hydrogenphosphate dihydrate and calcium oxalate monohydrate[46,51], indicating that a mass of carboxyl groups is insufficient to inhibit crystal growth and regulate the morphogenesis of struvite. It appears that the remarkable various effects can be attributed to the different molecule structures between PASP and aspartic acid. Using the circular dichroism technique, Addadi et al. confirmed that PASP with a molecular weight 6000 adopts a conformation comprising approximately 40% β-sheet and 60% random coil in Ca^{2+} solution[61]. The β-sheet conformation may favor the formation of more coordination bonds between PASP side chain carboxyl groups and magnesium cations exposed on the crystal face of struvite, and facilitate a structural and stereochemical fit between the distances of carboxylic groups in the PASP and the distances of neighboring magnesium cations from struvite crystal faces[46,48]. In this way, PASP binds tightly with the crystal faces and regulates struvite morphogenesis. However, recent studies also demonstrated that many mineral-associated proteins lack periodic structures even when adsorbed to crystals[62–64], and thus Hunter et al. proposed a flexible polyelectrolyte hypothesis of protein-biomineral interaction[64]. In this model, protein-crystal interactions essentially involve a general electrostatic attraction rather than structural complementarities between the protein conformation and the crystal face. Therefore, the different mineralization effects between PASP and aspartic acid can also be reasonably interpreted as a high negative density and conformation flexibility of PASP relative to aspartic acid. At the same time, a mass of carboxyl groups allows for effective complexation between PASP and Mg^{2+} in solution, resulting in the growth inhibition of struvite. Therefore, comparative experiments with PASP and aspartic acid may highlight the importance of molecule conformation in morphogenesis and the growth inhibition of struvite. Based on these findings, it can safely be concluded that both the component (e.g., carboxylic functional group) and structure (chain length and molecule conformation) lead to the high inhibitory effectiveness of PASP. Furthermore, it should be kept in mind that PASP is a structural and functional analogue of aspartic acid residues in acidic proteins while aspartic acid residues are important components of some key urinary proteins intimately involved in the pathological mineralization processes of urinary stones[18]. For example, osteopontin contains approximately 15–20% aspartic acid residues[24] and nephrocalcin contains approximately 11%[51]. Hence, we propose that aspartic acid residues or peptide chains in urinary proteins make an important contribution not only to the morphogenesis but also to the growth inhibition of the struvite stones.

Implication for pathological biomineralization

Struvite stones formed in human body tend to be staghorn-like structures while similar dendrites appear in bacterially induced mineralization experiments[11,26,28,33]. These branched struvite stones cause harm to the human body by blocking the urinary tract and damaging the urinary tract and kidneys[26]. Therefore, understanding the formation mechanism of these morphologies is important for treating urinary calculus. Although some investigations have proposed that the special morphologies depend on either supersaturation or growth kinetics, very few have implicated urinary proteins[26,27,33,35]. Recently, urinary proteomics has led to the iden-

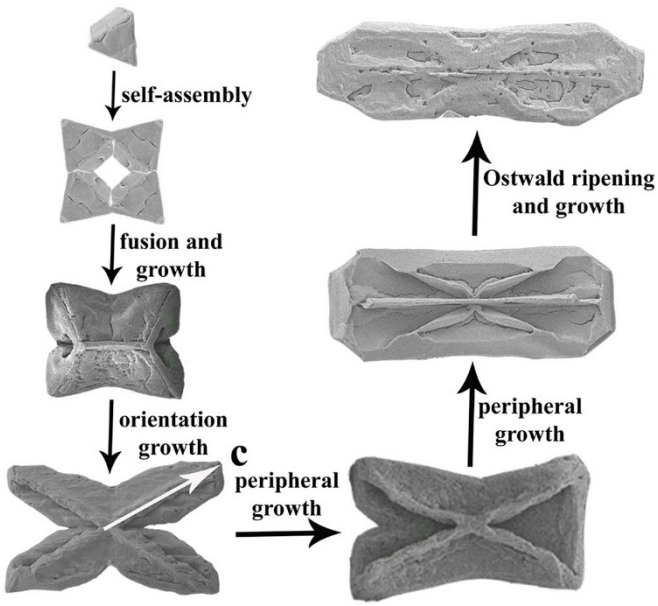

Figure 6 | Schematic illustration of the morphology evolution process of struvite in the presence of PASP.

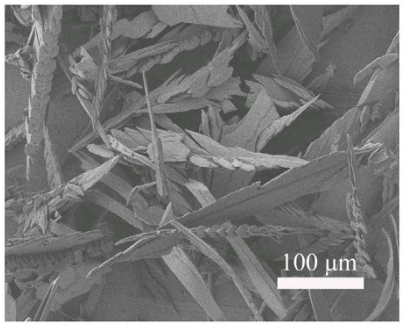

Figure 7 | FESEM image of the sample grown for 2 h in the presence of aspartic acid.

tification of thousands of proteins in urine where urinary stones form[65], and an increasing number of papers have revealed that urinary proteins play a key role in controlling the crystal growth of urinary stones[15,17,18,21,22]. In our case, PASP was chosen as a model peptide to investigate the impact of urinary proteins on struvite morphogenesis. Our time-resolved experiments indicate that PASP at a relatively low concentration can induce a series of specific morphologies of struvite. Interestingly, the obtained X-shaped crystals and crystals with unusual tabular habits are reminiscent of biogenic struvite morphologies[26,27,33,35,37,38]. We also find that these unique morphologies are not isolated from each other but temporally connected. Therefore this reveals the morphogenesis mechanism of biogenic struvite and emphasizes the importance of aspartic acid-rich urinary proteins on the morphological control of struvite. Moreover, in view of the complex components in urine, X-shaped struvite most likely develops into staghorn-like and dendritic stones after aggregation and assembly. For example, Prywer and Torzewska observed that X-shaped struvite crystals turn into dendrites in bacterial mineralization experiments[27]. In other words, staghorn calculi frequently occurring in the human body can be induced by aspartic acid-rich urinary proteins at a relatively low concentration. Concentration-dependent experiments show that PASP at a relatively high concentration can effectively inhibit struvite growth while aspartic acid monomers show no significant effect. Hence, urinary proteins may also exert an inhibitory capacity on struvite growth by means of their aspartic acid residues, in accordance with the finding that a number of inhibitory proteins are enriched with aspartic acid residues[16,18,21–24].

Taken together, our experiments indicate that aspartic acid residues in urinary proteins may exert either a positive or negative effect on struvite growth. That is, high concentration aspartic acid-rich proteins can effectively inhibit struvite growth. When the protein concentration is reduced by pathological changes or the incorporation in crystals of the growing stone, the inhibitory capacity will decrease accordingly[18]. What is worse, a relatively low protein concentration will induce the formation of staghorn-like and dendritic struvite stones. Similarly, the dual functional roles of proteins have been found in other cases[18,21,66]. For example, dentin phosphophoryn can act as an inhibitor of hydroxyapatite nucleation and growth in solution or can nucleate the formation of hydroxyapatite when adsorbed on a solid surface[21].

Indeed, concentration-dependent experiments have confirmed that PASP can effectively inhibit struvite growth. Previous studies have also reported that PASP had a similar inhibitory capacity on the crystal growth of calcium oxalate and calcium phosphate[46,50–53]. These three minerals make up the key components of urinary stones[10]. That is to say, PASP is a good inhibitor of urinary stone formation. Moreover, PASP can promote the dissolution of calcium oxalate and calcium phosphate due to its ability to chelate metal ions in solution[51,67]. We also found that PASP could be a driving force for struvite dissolution (data not shown). Therefore, PASP could accelerate the dissolution of urinary stones already existing in the human body. Moreover, PASP has excellent properties, including its water-solubility, nontoxic nature, biodegradability, and biocompatibility[54,68–70]. Therefore, PASP can potentially be developed into a therapeutic drug for urinary stone disease. As such, this study provides a new insight into the pathological biomineralization and a path toward the eventual design of therapeutic agents for urinary stone disease.

Methods

All starting chemicals were obtained commercially without further purification. Ammonia water ($NH_3 \cdot H_2O$), ammonium dihydrogen phosphate ($NH_4H_2PO_4$), magnesium chloride hexahydrate ($MgCl_2 \cdot 6H_2O$), sodium hydroxide (NaOH), poly-L-aspartic acid [($C_4H_5NO_3$) N] and L-aspartic acid ($C_4H_7NO_4$) were of analytical grade. In particular, PASP was purchased from Chengdu Ai Keda Chemical Technology Co., Ltd and the molecular weight was 5000. Deionized water was used in all our experiments.

The biomimetic growth of struvite was conducted in an ammonia diffusion system at room temperature. In a typical biomimetic synthesis, 0.05 g (0.01 mmol) of PASP and 0.0407 g (0.2 mmol) of $MgCl_2 \cdot 6H_2O$ were dissolved in a 50-mL beaker containing 50 mL deionized water with mild stirring, followed by the addition of 0.023 g (0.2 mmol) of $NH_4H_2PO_4$. After continuous stirring a homogeneous solution was obtained and the pH of the solution was adjusted to 7.0 using a diluted NaOH solution. The beaker was covered with stretched parafilm into which six needle holes were punched, and placed into a closed desiccator. A bottle (30 mL) of diluted ammonia water (5 mol/L) was also placed in the desiccator as a source of ammonia. After 8 h of mineralization, the product was isolated by centrifugation (1400 g for 3 minutes), cleaned by three cycles of centrifugation/washing/redispersion in deionized water and ethanol, to remove the organic components possibly adsorbed on the mineral surfaces, and allowed to dry at room temperature for 1 day. The same procedures were employed in a series of time-resolved experiments and PASP concentration-dependent experiments. Comparative experiments were also performed with the same procedure without PASP or using L-aspartic acid instead of PASP.

The morphology of the products was investigated by a JEOL JSM-6700F field emission scanning electron microscope (FESEM). Focused ion beam (FIB) analysis was conducted on the dual beam FIB/SEM system employing a FEI Helios NanoLab 650 microscope, equipped with a gallium ion source operating in an accelerating-voltage range 0.5–30 kV and an omniprobe™ micromanipulator. X-ray diffraction patterns (XRD) were recorded on a Japan MapAHF X-ray diffractometer equipped with Cu Kα irradiation ($\lambda = 0.154056$ nm). Infrared spectrum analysis was conducted on a Nicolet 8700 FT-IR spectrophotometer on KBr pellets. The products were further investigated by thermogravimetric and differential thermal analysis (TG-DTA) employing a SDTQ 600 TG/DTA thermal analyzer with a heating rate of 10°C/min from room temperature to 1000°C under air gas flow.

1. Addadi, L. & Weiner, S. Interactions between acidic proteins and crystals: stereochemical requirements in biomineralization. *Proc. Natl. Acad. Sci. USA* **82**, 4110–4114 (1985).
2. Addadi, L. & Weiner, S. Control and design principles in biological mineralization. *Angew. Chem. Int. Edit.* **31**, 153–169 (1992).
3. Skinner, H. C. W. Biominerals. *Mineral. Mag.* **69**, 621–641 (2005).
4. Wilt, F. H. Developmental biology meets materials science: morphogenesis of biomineralized structures. *Dev. Biol.* **280**, 15–25 (2005).
5. Weiner, S. Biomineralization: A structural perspective. *J. Struct. Biol.* **163**, 229–234 (2008).
6. Bazylinski, D. A. & Frankel, R. B. Biologically controlled mineralization in prokaryotes. *Rev. Mineral. Geochem.* **54**, 217–247 (2003).
7. Pósfai, M. & Dunin-Borkowski, R. E. Magnetic nanocrystals in organisms. *Elements* **5**, 235–240 (2009).
8. Weiner, S. Aspartic acid-rich proteins: major components of the soluble organic matrix of mollusk shells. *Calcified Tissue Int.* **29**, 163–167 (1979).
9. Addadi, L., Moradian, J., Shay, E., Maroudas, N. G. & Weiner, S. A chemical model for the cooperation of sulfates and carboxylates in calcite crystal nucleation: relevance to biomineralization. *Proc. Natl. Acad. Sci. USA* **84**, 2732–2736 (1987).
10. Griffith, D. P. Struvite stones. *Kidney Int.* **13**, 372–382 (1978).
11. Bichler, K. H. *et al*. Urinary infection stones. *Int. J. Antimicrob. Ag.* **19**, 488–498 (2002).
12. Coe, F. L., Evan, A. & Worcester, E. Kidney stone disease. *J. Clin. Invest.* **115**, 2598–2608 (2005).
13. Laird, D. F., Mucalo, M. R. & Yokogawa, Y. Growth of calcium hydroxyapatite (Ca-HAp) on cholesterol and cholestanol crystals from a simulated body fluid: a possible insight into the pathological calcifications associated with atherosclerosis. *J. Colloid Interf. Sci.* **295**, 348–363 (2006).
14. Portincasa, P., Moschetta, A. & Palasciano, G. Cholesterol gallstone disease. *Lancet* **368**, 230–239 (2006).
15. Fleisch, H. Inhibitors and promoters of stone formation. *Kidney Int.* **13**, 361–371 (1978).
16. Shiraga, H. *et al*. Inhibition of calcium oxalate crystal growth *in vitro* by uropontin: another member of the aspartic acid-rich protein superfamily. *Proc. Natl. Acad. Sci. USA* **89**, 426–430 (1992).
17. Ryall, R. L. Urinary inhibitors of calcium oxalate crystallization and their potential role in stone formation. *World J. Urol.* **15**, 155–164 (1997).
18. Khan, S. R. & Kok, D. J. Modulators of urinary stone formation. *Front. Biosci.* **9**, 1450–1482 (2004).
19. Qiu, S. R. *et al*. Molecular modulation of calcium oxalate crystallization by osteopontin and citrate. *Proc. Natl. Acad. Sci. USA* **101**, 1811–1815 (2004).
20. Grohe, B. *et al*. Control of calcium oxalate crystal growth by face-specific adsorption of an osteopontin phosphopeptide. *J. Am. Chem. Soc.* **129**, 14946–14951 (2007).
21. George, A. & Veis, A. Phosphorylated proteins and control over apatite nucleation, crystal growth and inhibition. *Chem. Rev.* **108**, 4670–4693 (2008).
22. Gower, L. B., Amos, F. F. & Khan, S. R. Mineralogical signatures of stone formation mechanisms. *Urol. Res.* **38**, 281–292 (2010).
23. Hoyer, J. R., Asplin, J. R. & Otvos, L. Phosphorylated osteopontin peptides suppress crystallization by inhibiting the growth of calcium oxalate crystals. *Kidney Int.* **60**, 77–82 (2001).

24. Chien, Y. C. *et al.* Modulation of calcium oxalate dihydrate growth by selective crystal-face binding of phosphorylated osteopontin and polyaspartate peptide showing occlusion by sectoral (compositional) zoning. *J. Biol. Chem.* **284**, 23491–23501 (2009).
25. D'Alessio, A. *et al.* An 8500-year-old bladder stone from Uzzo Cave (Trapani): Fourier transform-infrared spectroscopy analysis. *Archaeometry* **47**, 127–136 (2005).
26. Prywer, J. & Torzewska, A. Biomineralization of struvite crystals by *Proteus mirabilis* from artificial urine and their mesoscopic structure. *Cryst. Res. Technol.* **45**, 1283–1289 (2010).
27. Prywer, J. & Torzewska, A. Bacterially induced struvite growth from synthetic urine: experimental and theoretical characterization of crystal morphology. *Cryst. Growth Des.* **9**, 3538–3543 (2009).
28. Wall, I. & Tiselius, H. G. Studies on the crystallization of magnesium ammonium phosphate in urine. *Urol. Res.* **18**, 401–406 (1990).
29. Wang, Y. H. *et al.* Citrate and urease-induced crystallization in synthetic and human urine. *Urol. Res.* **21**, 109–115 (1993).
30. Mclean, R. J. C. & Nickel, J. C. Glycosaminoglycans and struvite calculi. *World J. Urol.* **12**, 49–51 (1994).
31. Romanowski, Z., Kempisty, P., Prywer, J., Krukowski, S. & Torzewska, A. Density functional theory determination of structural and electronic properties of struvite. *J. Phys. Chem. A* **114**, 7800–7808 (2010).
32. Chauhan, C. K. & Joshi, M. J. *In vitro* crystallization, characterization and growth-inhibition study of urinary type struvite crystals. *J. Cryst. Growth* **362**, 330–337 (2013).
33. Prywer, J., Torzewska, A. & Plocinski, T. Unique surface and internal structure of struvite crystals formed by *Proteus mirabilis*. *Urol. Res.* **40**, 699–707 (2012).
34. Abbona, F. & Boistelle, R. Growth morphology and crystal habit of struvite crystals ($MgNH_4PO_4{\cdot}6H_2O$). *J. Cryst. Growth* **46**, 339–354 (1979).
35. Mclean, R. J. C., Downey, J., Clapham, L. & Nickel, J. C. A simple technique for studying struvite crystal growth in vitro. *Urol. Res.* **18**, 39–43 (1990).
36. Asakura, H., Selengut, J. D., Orme-Johnson, W. H. & Dretler, S. P. The effect of calprotectin on the nucleation and growth of struvite crystals as assayed by light microscopy in real-time. *J. Urology* **159**, 1384–1389 (1998).
37. Prywer, J. & Torzewska, A. Effect of curcumin against *Proteus mirabilis* during crystallization of struvite from artificial urine. *Evidence-Based Compl. Alt. Med* **2012**, ID 862794 (2012).
38. Zhu, H. J. *et al.* The effect of plum juice on the prevention of struvite calculus formation *in vitro*. *BJU International.* **110**, E362–E367 (2012).
39. Chen, L. *et al.* Seed-mediated synthesis of unusual struvite hierarchical superstructures using bacterium. *Cryst. Growth Des.* **10**, 2073–2082 (2010).
40. Hugosson, J., Grenabo, L., Hedelin, H. & Pettersson, S. Effects of serum, albumin and immunoglobulins on urease-induced crystallization in urine. *Urol. Res.* **18**, 407–411 (1990).
41. Ebisuno, S., Komura, T., Yamagiwa, K. & Ohkawa, T. Urease-induced crystallizations of calcium phosphate and magnesium ammonium phosphate in synthetic urine and human urine. *Urol. Res.* **25**, 263–267 (1997).
42. Banks, E., Chianelli, R. & Korenstein, R. Crystal chemistry of struvite analogs of the type $MgMPO_4{\cdot}6H_2O$ ($M^+ = K^+$, Rb^+, Cs^+, Ti^+, NH_4^+). *Inorg. Chem.* **14**, 1634–1639 (1975).
43. Sun, B. J., Li, W. Z. & Wu, P. Y. Innovative spectral investigations on the thermal-induced poly (aspartic acid). *Polymer* **49**, 2704–2708 (2008).
44. Burke, E. M. *et al.* Influence of polyaspartic acid and phosphophoryn on octacalcium phosphate growth kinetics. *Colloid. Surface. B* **17**, 49–57 (2000).
45. Gower, L. B. & Odom, D. J. Deposition of calcium carbonate films by a polymer-induced liquid-precursor (PILP) process. *J. Cryst. Growth* **210**, 719–734 (2000).
46. Sikirić, M., Babić-Ivančić, V., Milat, O., Sarig, S. & Füredi-Milhofer, H. Factors influencing additive interactions with calcium hydrogenphosphate dihydrate crystals. *Langmuir* **16**, 9261–9266 (2000).
47. Roque, J., Molera, J., Vendrell-Saz, M. & Salvado, N. Crystal size distributions of induced calcium carbonate crystals in polyaspartic acid and *Mytilus edulis* acidic organic proteins aqueous solutions. *J. Cryst. Growth* **262**, 543–553 (2004).
48. Njegić-Džakula, B., Brečević, L., Falini, G. & Kralj, D. Calcite crystal growth kinetics in the presence of charged synthetic polypeptides. *Cryst. Growth Des.* **9**, 2425–2434 (2009).
49. Collins, I. R. Surface electrical properties of barium sulfate modified by adsorption of poly α, β aspartic acid. *J. Colloid Interf. Sci.* **212**, 535–544 (1999).
50. Beshensky, A. M. *et al.* Effects of urinary macromolecules on hydroxyapatite crystal formation. *J. Am. Soc. Nephrol.* **12**, 2108–2116 (2001).
51. Guo, S. W., Ward, M. D. & Wesson, J. A. Direct visualization of calcium oxalate monohydrate crystallization and dissolution with atomic force microscopy and the role of polymeric additives. *Langmuir* **18**, 4284–4291 (2002).
52. Sheng, X. X., Ward, M. D. & Wesson, J. A. Adhesion between molecules and calcium oxalate crystals: critical interactions in kidney stone formation. *J. Am. Chem. Soc.* **125**, 2854–2855 (2003).
53. Bigi, A. *et al.* Morphological and structural modifications of octacalcium phosphate induced by poly-L-aspartate. *Cryst. Growth Des.* **4**, 141–146 (2004).
54. Hasson, D., Shemer, H. & Sher, A. State of the art of friendly "green" scale control inhibitors: a review article. *Ind. Eng. Chem. Res.* **50**, 7601–7607 (2011).
55. Wu, Y. T. & Grant, C. Effect of chelation chemistry of sodium polyaspartate on the dissolution of calcite. *Langmuir* **18**, 6813–6820 (2002).
56. Wang, D. B., Wallace, A. F., De Yoreo, J. J. & Dove, P. M. Carboxylated molecules regulate magnesium content of amorphous calcium carbonates during calcification. *Proc. Natl. Acad. Sci. USA* **106**, 21511–21516 (2009).
57. Jiang, S. D., Yao, Q. Z., Zhou, G. T. & Fu, S. Q. Fabrication of hydroxyapatite hierarchical hollow microspheres and potential application in water treatment. *J. Phys. Chem. C* **116**, 4484–4492 (2012).
58. Wierzbicki, A., Sallis, J. D., Stevens, E. D., Smith, M. & Sikes, C. S. Crystal growth and molecular modeling studies of inhibition of struvite by phosphocitrate. *Calcified Tissue Int.* **61**, 216–222 (1997).
59. Zhou, G. T., Yao, Q. Z., Ni, J. & Jin, G. Formation of aragonite mesocrystals and implication for biomineralization. *Am. Mineral.* **94**, 293–302 (2009).
60. Yao, Q. Z., Guan, Y. B., Zhou, G. T. & Fu, S. Q. Witherite nanorods form mesocrystals: a direct experimental examination of a dipole-driven self-assembly model. *Eur. J. Mineral.* **24**, 519–526 (2012).
61. Addadi, L., Moradian-Oldak, J. & Weiner, S. [Macromolecule-crystal recognition in biomineralization]. *Surface Reactive Peptides and Polymers–Discovery and Commercialization* [Sikes, C. S. & Wheeler, A. P. (ed.)] [13–27] (American Chemical Society, Washington, D. C., 1991).
62. Fisher, L. W., Torchia, D. A., Fohr, B., Young, M. F. & Fedarko, N. S. Flexible structures of SIBLING proteins, bone sialoprotein, and osteopontin. *Biochem. Bioph. Res. Commun.* **280**, 460–465 (2001).
63. Evans, J. S. 'Apples' and 'oranges': comparing the structural aspects of biomineral- and ice-interaction proteins. *Curr. Opin. Colloid Interface Sci.* **8**, 48–54 (2003).
64. Hunter, G. K., O'Young, J., Grohe, B., Karttunen, M. & Goldberg, H. A. The Flexible polyelectrolyte hypothesis of protein-biomineral interaction. *Langmuir* **26**, 18639–18646 (2010).
65. Nagaraj, N. & Mann, M. Quantitative analysis of the intra- and inter-individual variability of the normal urinary proteome. *J. Proteome Res.* **10**, 637–645 (2011).
66. Campbell, A. A., Ebrahimpour, A., Perez, L., Smesko, S. A. & Nancollas, G. H. The dual role of polyelectrolytes and proteins as mineralization promoters and inhibitors of calcium oxalate monohydrate. *Calcified Tissue Int.* **45**, 122–128 (1989).
67. Poumier, F., Schaad, P., Haikel, Y., Voegel, J. C. & Gramain, P. Dissolution of synthetic hydroxyapatite in the presence of acidic polypeptides. *J. Biomed. Mater. Res.* **45**, 92–99 (1999).
68. Roweton, S., Huang, S. J. & Swift, G. Poly(aspartic acid): synthesis, biodegradation, and current applications. *J. Environ. Polym. Degr.* **5**, 175–181 (1997).
69. Thombre, S. M. & Sarwade, B. D. Synthesis and biodegradability of polyaspartic acid: a critical review. *J. Macromol. Sci. Pure A.* **42**, 1299–1315 (2005).
70. Dziak, K. L. & Akkus, O. Effects of polyelectrolytic peptides on the quality of mineral crystals grown in vitro. *J. Bone Miner. Metab.* **26**, 569–575 (2008).

Acknowledgments

This work was partially supported by the Chinese Ministry of Science and Technology (No. 2011CB808800), the Natural Science Foundation of China (No. 41272054), and the Specialized Research Fund for the Doctoral Program of Higher Education (No. 20133402130007). We would like to thank Dr. Lin-Jun Wang and Dr. Xiao-Lei Wen (USTC Center for Micro- and Nanoscale Research and Fabrication) for providing access to FIB equipment and for valuable discussions about the FIB data. We are also grateful to Dr. Jie-Jie Chen (Department of Chemistry, University of Science and Technology of China) for providing assistance on molecular modeling and for fruitful discussions.

Author contributions

H.L. conducted the experiments and wrote the main text. Q.Z.Y. designed the experiments and conducted the data analysis. Y.Y.W. performed the SEM experiments. Y.L.L. conducted the data analysis and revised the manuscript. G.T.Z. designed the experiments, conducted the data analysis and wrote the manuscript. All authors reviewed the manuscript.

Additional information

Supplementary information accompanies this paper at http://www.nature.com/scientificreports

Competing financial interests: The authors declare no competing financial interests.

How to cite this article: Li, H., Yao, Q.-Z., Wang, Y.-Y., Li, Y.-L. & Zhou, G.-T. Biomimetic synthesis of struvite with biogenic morphology and implication for pathological biomineralization. *Sci. Rep.* **5**, 7718; DOI:10.1038/srep07718 (2015).